

Multivariate Time-Series Anomaly Detection with Contaminated Data

Thi Kieu Khanh Ho ^{*}, Narges Armanfard

Department of Electrical and Computer Engineering, McGill University
Mila - Quebec AI Institute, Montreal, QC, Canada

Abstract

Mainstream unsupervised anomaly detection algorithms often excel in academic datasets, yet their real-world performance is restricted due to the controlled experimental conditions involving clean training data. Addressing the challenge of training with noise, a prevalent issue in practical anomaly detection, is frequently overlooked. In a pioneering endeavor, this study delves into the realm of label-level noise within sensory time-series anomaly detection (TSAD). This paper presents a novel and practical end-to-end unsupervised TSAD when the training data are contaminated with anomalies. The introduced approach, called TSAD-C, is devoid of access to abnormality labels during the training phase. TSAD-C encompasses three modules: a Decontaminator to rectify the abnormalities (aka noise) present in the training data, a Long-range Variable Dependency Modeling module to capture both long-term intra- and inter-variable dependencies within the decontaminated data that can be considered as a surrogate of the pure normal data, and an Anomaly Scoring module to detect anomalies from all types. Our extensive experiments conducted on three reliable datasets conclusively demonstrate that our approach surpasses existing methodologies, thus establishing a new state-of-the-art performance in the field.

1 Introduction

Multivariate time-series data (MTS) are referred to as time-stamped data that consists of multiple variables, i.e., for each timestamp, there are multiple values associated with it. Time-series anomaly detection (TSAD) is the process of detecting unusual patterns or events within time-series data that deviate from the expected behavior [Ho *et al.*, 2023]. The unusual patterns can be found in many real-world applications such as instances of financial fraud, abrupt temperature spikes or

unforeseen precipitation in weather data, security breaches, system malfunctions, and irregularities in heart rate or brain activities. Many algorithms have been proposed to automatically detect anomalies in time-series data [Su *et al.*, 2019; Shen *et al.*, 2020; Deng and Hooi, 2021; Li *et al.*, 2021; Chen *et al.*, 2022; Carmona *et al.*, 2022; Tang *et al.*, 2023; Ho and Armanfard, 2023; Hojjati *et al.*, 2023]. However, several critical challenges remain unresolved.

First, existing studies can be categorized into two groups, which are supervised methods utilizing both labeled normal and abnormal data in the training phase, and unsupervised methods assuming that only normal data is available during training. Given the demanding nature of accurately labeling anomalous patterns – proving to be time-consuming, costly, and labor-intensive – supervised approaches are deemed impractical. Consequently, there has been a recent surge in the development of unsupervised approaches. However, in many real-world applications, anomalies often sneak into normal data, which comes from the data shift or human misjudgment [Jiang *et al.*, 2022]. These unsupervised methods are sensitive to the seen anomalies due to their exhaustive strategy to model the normal training data, hence, they would misdetect similar anomaly samples in the test phase. Therefore, developing a method that can detect anomalies while being trained on contaminated data is necessary, yet there is no method that has aimed to tackle this challenge in the TSAD field (i).

Second, it is important to capture both intra-variable (aka temporal) and inter-variable (aka spatial) dependencies in MTS [Ho *et al.*, 2023]. However, existing unsupervised studies are unable to effectively capture them. Regarding the intra-variable dependencies, they often preprocessed data by segmenting the signals into short time intervals [Strothoff *et al.*, 2020; Pradhan *et al.*, 2022], or applied traditional temporal networks such as recurrent neural networks or transformers [Lim *et al.*, 2021; Katharopoulos *et al.*, 2020]. Such learned dependencies imply that observations close to each other are expected to be similar. This is problematic as trends, seasonality and unpredictability are always present in the time series. Thus, developing a method that can handle the *long-range* intra-variable dependencies to aid in distinguishing normal and abnormal variations in MTS is crucial (ii).

Regarding the inter-variable dependencies, very recently, graphs have brought the potential to model the relationships between variables (sensors) in time-series data. By represent-

^{*}Corresponding Author (Email: thi.k.ho@mcgill.ca).

This paper has been submitted for possible publication. Copyright may be transferred without notice, after which this version may no longer be accessible.

ing variables as nodes and their connections as edges, graphs provide an intuitive way to understand the underlying relationships between variables - a useful property in TSAD. For example, the changes in one variable can be used to predict the changes in another if they are correlated. However, modeling graphs to effectively capture this type of dependencies is challenging. Existing studies proposed to pre-define graphs based on prior knowledge, e.g., the known locations of sensors [Tang *et al.*, 2021]. However, in many real-world applications, pre-defining the graph properties such as node locations and node features is not practical due to dynamic testing environment – e.g., electroencephalogram sensor locations in comatose/epilepsy patients may vary depending on the brain damaged regions. Hence, instead of pre-defining graphs, dynamically learning the graph over time is highly desirable.

Lastly, while long-range intra- and inter-variable dependencies are both important for TSAD, designing an effective joint learning framework to capture both dependencies is yet challenging. Recent studies have shown that there are two groups of a combined model: time-and-graph and time-then-graph [Gao and Ribeiro, 2022]. A time-and-graph approach first constructs graphs and then embeds a temporal network. On the other hand, a time-then-graph framework first projects time-series data to a temporal network, the extracted temporal features are then used to model graphs. It is shown that compared to a time-and-graph framework, a time-then-graph approach achieves a significant improvement in classification and regression tasks [Gao and Ribeiro, 2022; Tang *et al.*, 2023]. Yet, till now, no study has explored the time-then-graph framework for unsupervised TSAD (iii).

Based on the above observations, we propose a novel approach, called TSAD-C, that addresses (i)-(iii) challenges. The main contributions of this paper are described as follows:

- We propose a novel *fully* unsupervised approach, namely TSAD-C, trained on contaminated data in an end-to-end manner to detect anomalies in MTS. To the best of our knowledge, this is the first study that uses contaminated data in the training phase for TSAD, addressing a much more challenging problem than the existing studies.
- TSAD-C is comprised of three modules, namely Decontaminator, Long-range Variable Dependency Modeling, and Anomaly Scoring. The initial module aims to identify and eliminate abnormal patterns that are likely to be anomalies. The second module is a time-then-graph approach that is designed to model the long-term intra- and inter-variable dependencies. The last module computes anomaly scores to detect anomalies.
- The Decontaminator leverages masking strategies and an S4-based conditional diffusion model, while the Long-range Variable Dependency Modeling module integrates Intra-variable Modeling, and Inter-variable Modeling components. The Anomaly Scoring module leverages the insights of the first two modules.
- We perform extensive experiments on three widely used physiological datasets and demonstrate that our method outperforms existing studies and thus establishes a new state-of-the-art (SOTA) in the field.

2 Proposed Method

A dataset is defined as $X = (\mathbf{x}_{(1)}, \mathbf{x}_{(2)}, \dots, \mathbf{x}_{(N)})$, where $\mathbf{x}_{(i)} = (x_{(i)}^1, x_{(i)}^2, \dots, x_{(i)}^K)$ is the i th observation in the time series of N observations, $\mathbf{x}_{(i)} \in \mathbb{R}^{K \times L}$, K and L denote the number of variables (sensors) and the length of the i th observation, respectively. An observation can be conceptualized as L samples collected from K sensors over the i th time interval. Our task is to detect anomalous observations from all types in the test data (i.e., X_{test}) by training the model with contaminated data (i.e., X_{train}). Note that, during the training phase, no information about the outlier data that contaminates the normal data is provided, such as their labels or their positions within the time series. We use a validation set (i.e., X_{valid}) for early stopping and finding the decision threshold. The block diagram of the proposed TSAD-C method, depicting the three modules, namely Decontaminator, Long-range Variable Dependency Modeling, and Anomaly Scoring, is shown in Figure 1. Details of each module are presented below.

2.1 Decontaminator

Masking Strategies. Following the practical scenarios when collecting normal data, in this paper, we assume that the number of normal samples significantly outweighs the number of abnormal events. When masking a portion of X_{train} , there is a likelihood of removing both abnormal and normal patterns. Nonetheless, due to the predominant presence of normal data in X_{train} , the omission of certain normal patterns is not likely to yield detrimental consequences as the substantial amount of remaining normal data can adequately compensate for the masked portions. Conversely, the act of masking has the advantageous outcome of diminishing the proportion of anomalies. This effect is beneficial for the downstream module as it facilitates the learning process of variable dependencies that characterize the underlying behavior of normality.

We define a binary mask as $\mathbf{v} \in \{0, 1\}$, $\mathbf{v} \in \mathbb{R}^{K \times L}$, where zeros denote the values to be masked and the values to be kept are marked by ones. Hence, the i th masked observation is $\mathbf{x}_{(i)}^u = \mathbf{x}_{(i)} \odot \mathbf{v}$, where $\mathbf{x}_{(i)}^u \in \mathbb{R}^{K \times L}$ and \odot denotes point-wise multiplication. Following the literature of masking techniques [Khayati *et al.*, 2020; Alcaraz and Strodthoff, 2022], we perform three popular masking scenarios, namely random masking (RandM), random block masking (RandBM) and blackout masking (BoM). A hyperparameter, called the number of time stamps r , is assigned for three masking methods. RandM randomly samples r to be masked across variables (sensors). In RandBM, there might be no time overlap between the masked windows across variables, whereas in BoM, the same time window is masked across all variables. Note that each window has the size of r .

S4-based Conditional Diffusion Model. This module is developed based on a diffusion model, a class of generative models inspired by non-equilibrium thermodynamics [Sohl-Dickstein *et al.*, 2015]. It defines a two-process paradigm, including the diffusion and reserve processes. In this paper, the diffusion process, defined by a Markov chain, incrementally adds Gaussian noise to the initial stage of $\mathbf{x}_{(i)}^u$, called

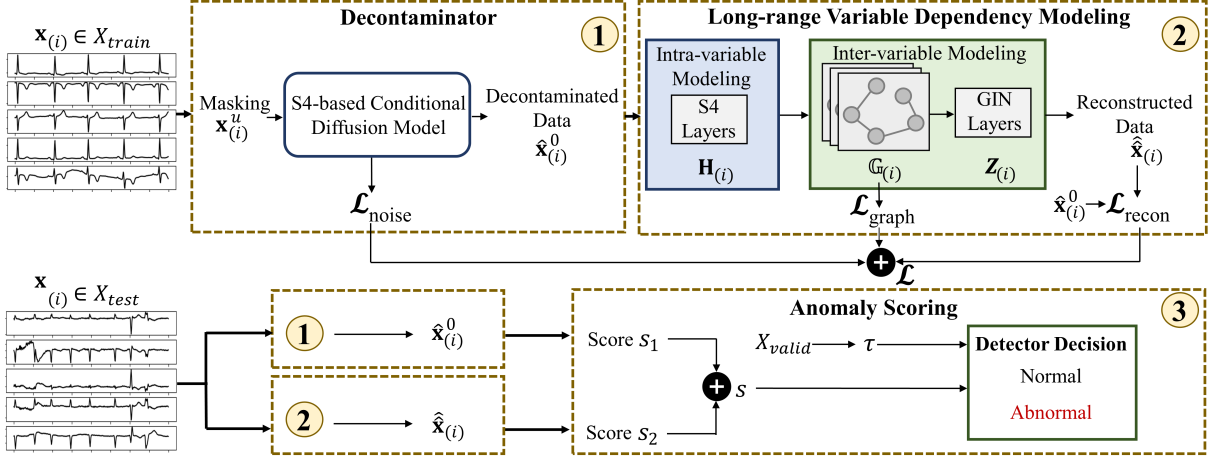


Figure 1: The overall framework of TSAD-C.

$\mathbf{x}_{(i)}^0$, over T diffusion steps and can be represented as:

$$p(\mathbf{x}_{(i)}^1, \dots, \mathbf{x}_{(i)}^T | \mathbf{x}_{(i)}^0) = \prod_{t=1}^T p(\mathbf{x}_{(i)}^t | \mathbf{x}_{(i)}^{t-1}), \quad (1)$$

where $p(\mathbf{x}_{(i)}^t | \mathbf{x}_{(i)}^{t-1}) := \mathcal{N}(\mathbf{x}_{(i)}^t; \mu_{(i)}^t, \sigma_{(i)}^t)$. This indicates $\mathbf{x}_{(i)}^t$ is sampled from a normal distribution with mean $\mu_{(i)}^t = \sqrt{1 - \beta_t} \mathbf{x}_{(i)}^{t-1}$ and variance $\sigma_{(i)}^t = \beta_t \mathbf{I}$. \mathbf{I} is the identity matrix, $\beta_t \in (0, 1)$ is a variance schedule that controls the quantity of noise added at the t th diffusion step. In our implementation, we increase β_t linearly from 10^{-4} to 0.02. By setting $\alpha_t = 1 - \beta_t$, $\bar{\alpha}_t = \prod_{j=1}^t \alpha_j$, the diffusion process allows to immediately transform $\mathbf{x}_{(i)}^0$ to a noisy $\mathbf{x}_{(i)}^t$ according to β_t in a closed form as $\mathbf{x}_{(i)}^t = \sqrt{\bar{\alpha}_t} \mathbf{x}_{(i)}^0 + \sqrt{1 - \bar{\alpha}_t} \epsilon_t$ where the noise $\epsilon_t \sim \mathcal{N}(0, \mathbf{I})$, $\epsilon_t \in \mathbb{R}^{K \times L}$. We add noise to both masked and non-masked portions of $\mathbf{x}_{(i)}^0$. As the diffusion step increases, $\mathbf{x}_{(i)}^0$ gradually loses its distinguishable features and approaches a Gaussian distribution; hence, both anomalous and normal patterns appear indistinguishable.

The reverse process defined by a Markov chain is parameterized by θ and can be represented as:

$$q_{\theta}(\mathbf{x}_{(i)}^0, \dots, \mathbf{x}_{(i)}^{T-1} | \mathbf{x}_{(i)}^T) = \prod_{t=1}^T q_{\theta}(\mathbf{x}_{(i)}^{t-1} | \mathbf{x}_{(i)}^t), \quad (2)$$

where each $q_{\theta}(\mathbf{x}_{(i)}^{t-1} | \mathbf{x}_{(i)}^t) := \mathcal{N}(\mathbf{x}_{(i)}^{t-1}; \mu_{\theta}(\mathbf{x}_{(i)}^t, t, c), \sigma_{\theta}(\mathbf{x}_{(i)}^t, t, c)^2 \mathbf{I})$. μ_{θ} and σ_{θ} are parameterized as:

$$\begin{aligned} \mu_{\theta}(\mathbf{x}_{(i)}^t, t, c) &= \frac{1}{\sqrt{\alpha_t}} \left(\mathbf{x}_{(i)}^t - \frac{\beta_t}{\sqrt{1 - \alpha_t}} \epsilon_{\theta}(\mathbf{x}_{(i)}^t, t, c) \right), \\ \sigma_{\theta}(\mathbf{x}_{(i)}^t, t, c) &= \sqrt{\beta_t}, \end{aligned} \quad (3)$$

where $\bar{\beta}_t = \frac{1 - \bar{\alpha}_{t-1}}{1 - \bar{\alpha}_t} \beta_t$ and $\bar{\beta}_1 = \beta_1$. ϵ_{θ} is a network approximator, which takes $\mathbf{x}_{(i)}^t$, the diffusion step t and a conditional factor c as the inputs and aims to predict the noise from $\mathbf{x}_{(i)}^t$. Note that compared to the unconditional diffusion models,

conditional cases typically achieve a better performance as the reverse process is conditioned on additional information [Alcaraz and Strodthoff, 2022]. In our scenario, c is a concatenation of the non-masked segments in $\mathbf{x}_{(i)}^u$ and the positional information of the masked parts provided by \mathbf{v} . With this extra information, it facilitates the reverse process to distinguish the zero portions of non-masked and masked parts. It is worth mentioning that ϵ_{θ} has an important role in the reverse process. U-Net-like architectures, based on PixelCNN and ResNet, are typically utilized to build ϵ_{θ} for anomaly detection in the image domain [Zhang *et al.*, 2023]. However, in the time-series domain, capturing long-range intra-variable dependencies is crucial. Hence, we propose to build ϵ_{θ} based on a recently proposed deep sequence model, called S4 [Gu *et al.*, 2022]. S4 is basically based on the concept of a state space model (SSM). A continuous-time SSM maps $\mathbf{x}_{(i)}^t$ to a high dimensional state $h_{(i)}^t$ before projecting it to the output $\mathbf{y}_{(i)}^t$. This transition can be defined as:

$$\dot{h}_{(i)}^t = A h_{(i)}^t + B \mathbf{x}_{(i)}^t \text{ and } \mathbf{y}_{(i)}^t = C h_{(i)}^t + D \mathbf{x}_{(i)}^t, \quad (4)$$

where A, B, C, D are transition matrices learned by gradient descent. S4 shows that a discrete-time SSM can be represented as a convolution operation by:

$$\bar{O} := (\bar{C}\bar{B}, \bar{C}\bar{A}\bar{B}, \dots, \bar{C}\bar{A}^{L-1}\bar{B}), \mathbf{y}_{(i)} = \bar{O} * \mathbf{x}_{(i)}, \quad (5)$$

where $\bar{A}, \bar{B}, \bar{C}$ are the discretized matrices, $\bar{C}\bar{A}^{L-1}$ denotes the multiplication of discretized matrices at $L - 1$, and \bar{O} is a SSM convolution kernel. Note that D is omitted in Equation (5) as $D\mathbf{x}_{(i)}^t$ can be viewed as a skip connection. Essentially, S4 parameterizes A as a diagonal plus low rank matrix and this parameterization enables fast computation of \bar{O} . Moreover, it includes the HiPPO matrices [Gu *et al.*, 2020], which are a series of matrices that is capable of capturing long-term intra-variable dependencies. Our Decontaminator module employs two S4 layers, one after the addition of the embeddings related to $\mathbf{x}_{(i)}^u$ and another layer after including c in the residual blocks (see Figure 2).

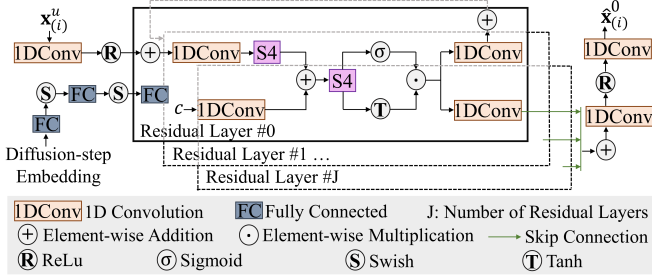


Figure 2: The architecture of the Decontaminator.

For a simpler and more streamlined reverse process during the training of ϵ_θ for noise estimation, we suggest minimizing the noise error specifically on the masked segments, as illustrated in Equation (6). It is important to highlight that the masked parts solely consist of noise without any underlying data pattern, unlike the non-masked parts which contain both noise and the actual data pattern. Consequently, deriving noise estimates from the masked data is a more straightforward task and can be accomplished using less intricate networks. This approach is advantageous as it facilitates swift data preparation for the subsequent module.

$$\mathcal{L}_{\text{noise}} = \|\epsilon_t \odot (1 - M) - \hat{\epsilon}_t \odot (1 - M)\|^2, \quad (6)$$

where $\hat{\epsilon}_t$ is the predicted noise obtained from $\epsilon_\theta(\mathbf{x}_{(i)}^t, t, c)$.

We obtain decontaminated data in the training phase as:

$$\hat{\mathbf{x}}_{(i)}^0 = \frac{1}{\sqrt{\alpha_T}} \left(\mathbf{x}_{(i)}^T - \sqrt{1 - \alpha_T} \hat{\epsilon}_T \right). \quad (7)$$

Note that approximating $\hat{\mathbf{x}}_{(i)}^0$ immediately at the T th step allows us to have a faster reverse speed in the training phase as $\hat{\mathbf{x}}_{(i)}^0$ will be used as the input for the second module in the training framework. On the other hand, in the test phase, we perform a complete sampling step from T to 1 in the reverse process according to Equations (2) and (3) to obtain $\hat{\mathbf{x}}_{(i)}^0$.

2.2 Long-range Variable Dependency Modeling

In this module, we aim to build a time-then-graph framework, as is motivated in the Introduction, by incorporating two components, namely Intra-variable Modeling and Inter-variable Modeling. Details of each component are shown below.

Intra-variable Modeling. We propose to use multiple back-to-back S4 layers to capture long-range intra-variable dependencies. Specifically, we use $\hat{\mathbf{x}}_{(i)}^0 \in \mathbb{R}^{K \times L}$ as the input and project it onto an embedding space, called $\mathbf{H}_{(i)} \in \mathbb{R}^{K \times \Gamma \times U}$, where Γ and U are hyper-parameters defining the S4 embedding dimension. In our experiments, to maintain a sense of the number of time stamps present in $\mathbf{x}_{(i)}$, we set Γ to L , corresponding to the length of the input time series. This allows us to model the long-term intra-variable dependencies within each variable. $\mathbf{H}_{(i)}$ is used as the input to the graph learning phase, which models the underlying inter-variable dependencies. Prior studies have shown the superior performance of graph learning when using the temporal embedding rather than the original data [Tang *et al.*, 2023].

Inter-variable Modeling. To this end, we represent $\mathbf{H}_{(i)}$ as a set of graphs $\mathbb{G}_{(i)} = \{\mathcal{G}_{(i)}^m\}_{m=1}^d$, where $d = \frac{\Gamma}{g}$ and g is the pre-defined length of the short and non-overlapping time intervals within the i th observation. As each observation within a dataset can encompass thousands of time stamps, constructing a graph for every individual time step becomes inefficient and computationally demanding. A more effective approach involves creating a graph over a defined time interval, which aids in information aggregation. This strategy not only leads to a graph with reduced noise but also facilitates faster computations [Gao and Ribeiro, 2022].

We define $\mathcal{G}_{(i)}^m = \{\mathbf{E}_{(i)}^m, \mathcal{A}_{(i)}^m\}$. Here, $\mathbf{E}_{(i)}^m \in \mathbb{R}^{K \times U}$ represents the embedding derived by averaging the elements of $\mathbf{H}_{(i)}$ along its second dimension, and $\mathcal{A}_{(i)}^m \in \mathbb{R}^{K \times K}$ is the adjacency matrix. Each row and column in $\mathcal{A}_{(i)}^m$ corresponds to a node (i.e., variable). The non-zero value in the entry of $\mathcal{A}_{(i)}^m$ indicates that there exists an edge connecting the two corresponding nodes. To determine the edge weights, we employ a self-attention paradigm [Vaswani *et al.*, 2017; Tang *et al.*, 2023] in which attention weights are assigned to the edges' magnitudes. This process can be formulated as:

$$\mathbf{Q} = \mathbf{E}_{(i)}^m \mathbf{W}^{\mathbf{Q}}, \mathbf{R} = \mathbf{E}_{(i)}^m \mathbf{W}^{\mathbf{R}}, \quad (8)$$

$$\mathcal{A}_{(i)}^m = \text{softmax}\left(\frac{\mathbf{Q}\mathbf{R}^\top}{\sqrt{D}}\right),$$

where $\mathbf{W}^{\mathbf{Q}}, \mathbf{W}^{\mathbf{R}} \in \mathbb{R}^{U \times U}$ are the learnable weights that project $\mathbf{E}_{(i)}^m$ to the query \mathbf{Q} and the key \mathbf{R} , respectively.

In addition to the learnable parameters for creating the adjacency matrix $\mathcal{A}_{(i)}^m$, we include another pre-defined adjacency matrix, called $\mathcal{A}_{(i)}^m$ based δ -nearest neighbors to help guiding the graph learning process. Its edge magnitudes are computed by measuring the cosine similarity between the nodes' embeddings in $\mathbf{E}_{(i)}^m$. We only keep the top δ edges that have the highest values for each node to avoid overly connected graphs. In all our experiments, $\delta = 3$. The final $\mathcal{A}_{(i)}^m$ employed in the loss function is obtained as:

$$\mathcal{A}_{(i)}^m = \zeta \mathcal{A}_{(i)}^m + (1 - \zeta) \mathcal{A}_{(i)}^m, \quad (9)$$

where $\zeta \in [0, 1)$ is a hyper-parameter to balance the two contributing components.

Following the graph literature [Zhu *et al.*, 2021], it is important to have a graph regularized, i.e., to encourage a learnable graph to have desired graph properties such as smoothness (i.e., the features should change smoothly between neighboring nodes), sparsity (i.e., avoiding to have an overly connected graph) and connectivity (i.e., avoiding to have a disconnected graph). Hence, we include three constraints in the regularization loss as below:

$$\mathcal{L}_{\text{graph}} = \frac{1}{d} \sum_{m=1}^d \xi_1 \mathcal{L}_{\text{smooth}}(\mathbf{E}_{(i)}^m, \mathcal{A}_{(i)}^m) + \xi_2 \mathcal{L}_{\text{sparse}}(\mathcal{A}_{(i)}^m) + \xi_3 \mathcal{L}_{\text{connect}}(\mathcal{A}_{(i)}^m), \quad (10)$$

where $\mathcal{L}_{\text{smooth}} = \frac{1}{K^2} \text{tr}(\mathbf{E}_{(i)}^m \mathbf{M}_{\text{Lap}} \mathbf{E}_{(i)}^m)$, $\mathbf{M}_{\text{Lap}} = \mathbf{M}_{\text{degree}} - \mathcal{A}_{(i)}^m$ is the Laplacian matrix, $\mathbf{M}_{\text{degree}}$ is the degree matrix of $\mathcal{A}_{(i)}^m$, and $\text{tr}(\cdot)$ denotes the trace of the matrix. $\mathcal{L}_{\text{sparse}} =$

$\frac{1}{K^2} \|\mathcal{A}_{(i)}^m\|_F^2$ and $\|\cdot\|_F$ is the Frobenius norm of the matrix. $\mathcal{L}_{\text{connect}} = -\frac{1}{K} \mathbf{1}^\top \log(\mathcal{A}_{(i)}^m \cdot \mathbf{1})$, and $\mathbf{1} \in \mathbb{R}^{K \times 1}$ is a matrix of ones. ξ_1, ξ_2 and ξ_3 are hyper-parameters to balance the regularization terms in $\mathcal{L}_{\text{graph}}$.

We then propose to capture the inter-variable dependencies between nodes in $\mathcal{G}_{(i)}^m$ by utilizing a graph isomorphism network (GIN) [Xu *et al.*, 2019]. Note that GIN is a variant of graph neural networks (GNN) that shows a strong representational power compared to other types of GNN. The embedding of nodes in $\mathcal{G}_{(i)}^m$ is represented as $\mathbf{z}_{(i)}^m := \text{GIN}(\mathbf{E}_{(i)}^m, \mathcal{A}_{(i)}^m)$, $\mathbf{z}_{(i)}^m \in \mathbb{R}^{K \times g \times U}$. We concatenate the node embeddings of all graphs within $\mathbb{G}_{(i)}$ as $\mathbf{Z}_{(i)} = \text{concat}(\mathbf{z}_{(i)}^1, \dots, \mathbf{z}_{(i)}^d)$.

Finally, a linear layer is added to obtain reconstructed data $\hat{\mathbf{x}}_{(i)}$, i.e., $\hat{\mathbf{x}}_{(i)} := \text{Linear}(\mathbf{Z}_{(i)})$, $\hat{\mathbf{x}}_{(i)} \in \mathbb{R}^{K \times L}$. Thus, the reconstruction loss is denoted as:

$$\mathcal{L}_{\text{recon}} = \|\hat{\mathbf{x}}_{(i)}^0 - \hat{\mathbf{x}}_{(i)}\|^2. \quad (11)$$

The final loss in the training phase is defined as the total loss of all three losses from Equations (6), (10) and (11):

$$\mathcal{L} = \mathcal{L}_{\text{noise}} + \mathcal{L}_{\text{graph}} + \mathcal{L}_{\text{recon}}. \quad (12)$$

2.3 Anomaly Scoring

In the test phase, we compute an anomaly score based root mean square error (RMSE) for each observation $\mathbf{x}_{(i)}$. More specifically, we project $\mathbf{x}_{(i)}$ to the Decontaminator where masking strategies and the complete sampling step from T to 1 are applied to obtain $\hat{\mathbf{x}}_{(i)}^0$. If $\mathbf{x}_{(i)}$ is an abnormal observation, the masked portions are expected to be inaccurately sampled. At the same time, instead of using $\hat{\mathbf{x}}_{(i)}^0$ as the input for the second module as is done in the training phase, $\mathbf{x}_{(i)}$ is directly used to obtain $\hat{\mathbf{x}}_{(i)}$ in the test phase. The underlying assumption is that if $\mathbf{x}_{(i)}$ is an anomaly, the second component with the goal of achieving the flawless reconstruction of normal patterns would be unable to reconstruct it. The final score s for each $\mathbf{x}_{(i)}$ is computed as:

$$\begin{aligned} s_1 &= \left(\frac{1}{L} \sum_{l=1}^L \sum_{k=1}^K \left((\hat{\mathbf{x}}_{(i)}^0 - \mathbf{x}_{(i)}) \odot (1 - M) \right)^2 \right)^{0.5}, \\ s_2 &= \left(\frac{1}{L} \sum_{l=1}^L \sum_{k=1}^K \left(\hat{\mathbf{x}}_{(i)} - \mathbf{x}_{(i)} \right)^2 \right)^{0.5}, \\ s &= \lambda_1 s_1 + \lambda_2 s_2, \end{aligned} \quad (13)$$

where s_1 and s_2 are, respectively, the RMSE scores obtained from the first and second modules. λ_1 and λ_2 are hyper-parameters defined to ensure that anomaly scores from both modules fall within a similar numeric range. For a fair comparison, λ_1 and λ_2 are fixed in all our experiments and are the same across all datasets.

We conduct a decision threshold search on the *unlabeled* X_{valid} , deviating from the conventional TSAD practice where the decision threshold is typically selected on a *labeled* test set [Carmona *et al.*, 2022; Chen *et al.*, 2022]. This conventional approach often leads to biased and impractical performance, not aligned with real-world unsupervised applications where there no labeled data is available. We determine the

threshold, denoted as τ , through a quantile-based approach [Kuan *et al.*, 2017] applied to the anomaly scores obtained from the unlabeled X_{valid} . Specifically, we select a quantile corresponding to a rough estimation of the percentage of normal data in the X_{train} (and X_{valid}) dataset, as provided by the dataset provider. For instance, if approximately 20% of the data is deemed contaminated, we set the quantile threshold to 80%. In the test phase, observations with s above τ are detected as anomalies. Note that there is no overlap between X_{train} , X_{valid} , and X_{test} .

3 Experiments

3.1 Experimental Settings

In this section, we introduce the datasets and the experimental setup in our study.

Datasets. Numerous TSAD methods have relied on various benchmark datasets such as Yahoo, NASA, SWaT, WADI, SMAP, MSL and SMD. However, recent critiques suggest that these benchmarks are flawed and contribute to an illusion of progress [Wagner *et al.*, 2023], rendering them unsuitable for evaluating and comparing TSAD methods. To address this concern, our study opts for three publicly available, reliable, and challenging physiological datasets, which contain various types of anomalies and are annotated by a consensus of multiple experienced doctors. These include ICBEB [Liu *et al.*, 2018], DODH [Guillot *et al.*, 2020] and TUSZ [Shah *et al.*, 2018].

Specifically, ICBEB is an electrocardiogram database that includes the normal heart rhythm and different types of abnormalities. We select five anomaly types, namely atrial fibrillation, first-degree atrioventricular block, right bundle branch block, premature ventricular contraction and ST-segment elevation. DODH is a sleep staging database recorded from healthy volunteers. We select N3, which is the deepest sleeping stage, as normal data since the brain activity during this stage has an identifiable pattern of delta waves; and body activities such as breathing and muscle tone rate decrease. Meanwhile, rapid eye movement and awake stages are considered abnormal since the brain activity during these periods rises up; and the body activities such as the eyes and the muscles increase. TUSZ is an electroencephalogram database recorded from epilepsy patients. The resting-state brain activities are considered normal while abnormal brain activities are seizures. Details of each dataset are shown in Table 1. Note that we include approximately 20% of anomalies from all types in X_{train} and X_{valid} of each dataset to contaminate normal data during training, thereby increasing the challenge for any algorithm to detect all anomaly types in the test phase.

Baselines. We compare TSAD-C against nine SOTA unsupervised methods from the TSAD literature. We categorize the compared methods into three groups based on their ability to capture either intra-, inter-, or both-variable dependencies. Specifically, methods addressing intra-variable dependencies include LSTM-Autoencoder (LSTM-AE) [Wei *et al.*, 2023] and S4-Autoencoder (S4-AE) [Gu *et al.*, 2022]. Those handling inter-variable dependencies are Graph Autoencoder (GAE) [Du *et al.*, 2022], GDN [Deng and Hooi, 2021], and EEG-CGS [Ho and Armanfard, 2023]. Methods addressing

Dataset	$X_{\text{train}} (\eta)$	$X_{\text{valid}} (\eta)$	$X_{\text{test}} (\eta)$	K	L
ICBEB	910 (20.0%)	82 (20.7%)	222 (59.9%)	12	6,000
DODH	2515 (19.8%)	320 (21.8%)	310 (51.6%)	16	7,500
TUSZ	5275 (17.0%)	1055 (20.0%)	1581 (40.0%)	19	12,000

Table 1: The numbers of observations are shown in X_{train} , X_{valid} , X_{test} of each dataset. The anomaly ratio, denoted as η , is shown in parenthesis. K and L are, respectively, the number of variables and the length of an observation.

both types of dependencies include InterFusion [Li *et al.*, 2021], DVGCRN [Chen *et al.*, 2022], Gated Recurrent Unit-GNN (GRU-GNN), GraphS4mer [Tang *et al.*, 2023], and our proposed method. Note that, to ensure a fair comparison, we employ the same strategy of threshold finding based on the unlabeled X_{valid} for TSAD-C and all the compared methods.

Performance Evaluation Metrics. Given the utilization of the imbalanced datasets detailed in Table 1 across all methods, we employ three evaluation metrics, namely F1-score (F1), Recall (Rec), and Area Under the Precision-Recall curve (APR) [Davis and Goadrich, 2006], to comprehensively assess the performance of each method.

3.2 Comparison with SOTA

The performances of TSAD-C and existing methods are presented in Table 2. Note that TSAD-C uses RandBM in the Table. It shows that TSAD-C surpasses all existing studies and establishes a new SOTA in the field. Note that F1 shows the harmonic mean of precision and recall that considers both false positives and false negatives. A higher F1 score indicates that the model has a better balance between correctly detecting positive samples (i.e., anomalies), while effectively avoiding false positives. It also confirms that we obtain a significant improvement in Rec (i.e., the ability to correctly detect most of the abnormal cases) compared to the existing methods. This improvement is crucial when dealing with contaminated data, where existing unsupervised methods failed to detect the types of anomalies similar to those encountered during training due to their assumption of clean training data, leading to misdetection of such anomalies. It is also important to emphasize the significance of high F1 and Rec scores in real-world applications, especially in medical diagnosis and clinical settings. The preference for these scores stems from the model’s capability to flag potential abnormal cases for further examination by medical experts. This proactive approach helps in determining the appropriate course of action, thereby minimizing the risk of overlooking abnormal cases, which could otherwise result in delayed treatment or missed opportunities for early intervention.

3.3 Resilience to Contamination Levels

In this section, we verify the TSAD-C’s performance by conducting two additional settings of experiments on ICBEB: (1) changing the number of anomaly types and (2) changing the anomaly ratio, i.e., η , available in X_{train} and X_{valid} .

Variability on The Anomaly Types. We assess the TSAD-C’s performance in detecting the five anomaly types available in X_{test} while not all anomaly types are present in X_{train} and X_{valid} . To this end, we introduce κ as the number

	Method	Metric	ICBEB	DODH	TUSZ
Intra-	LSTM-AE	F1	0.609	0.534	0.471
		{Rec; APR}	{0.651; 0.752}	{0.706; 0.643}	{0.424; 0.592}
Intra-	S4-AE	F1	0.664*	0.625*	0.527
		{Rec; APR}	{0.735; 0.749}	{0.881; 0.713}	{0.576; 0.615}
Inter-	GAE	F1	0.575	0.480	0.508
		{Rec; APR}	{0.454; 0.746}	{0.613; 0.604}	{0.476; 0.625}
Inter-	GDN	F1	0.586	0.524	0.456
		{Rec; APR}	{0.515; 0.741}	{0.687; 0.636}	{0.398; 0.585}
Inter-	EEG-CGS	F1	0.561	0.502	0.516
		{Rec; APR}	{0.470; 0.740}	{0.650; 0.620}	{0.490; 0.619}
Both-	InterFusion	F1	0.649	0.418	0.532*
		{Rec; APR}	{0.651; 0.753}	{0.512; 0.559}	{0.520; 0.628}
Both-	GRU-GNN	F1	0.647	0.587	0.506
		{Rec; APR}	{0.689; 0.742}	{0.806; 0.684}	{0.474; 0.613}
Both-	DVGCRN	F1	0.615	0.480	0.397
		{Rec; APR}	{0.575; 0.744}	{0.612; 0.604}	{0.322; 0.554}
Both-	GraphS4mer	F1	0.638	0.565	0.524
		{Rec; APR}	{0.667; 0.738}	{0.762; 0.667}	{0.511; 0.621}
Both-	Ours	F1	0.707	0.652	0.545
		{Rec; APR}	{0.841; 0.773}	{0.843; 0.728}	{0.830; 0.652}

Table 2: Comparison between existing methods and ours. The best and second-best F1 scores are denoted in bold and *.

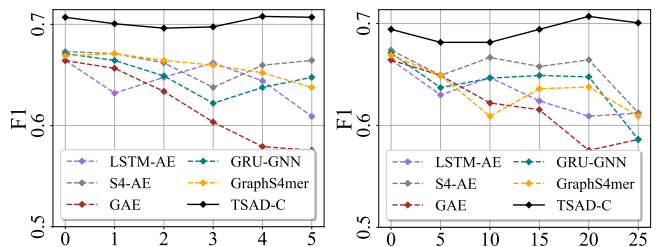


Figure 3: **(Left)** F1 Score Versus The Number of Anomaly Types (i.e., κ). **(Right)** F1 Score Versus The Anomaly Ratio (i.e., η).

of anomaly types – e.g., $\kappa = 2$ signifies two anomaly types present in X_{train} and X_{valid} . Note that the anomaly ratio in X_{train} and X_{valid} remain constant. Figure 3 **(Left)** shows that the performance of unsupervised methods diminishes as κ increases since they all assume the given input data as pure normal data, hence are incapable of handling contaminated data. These methods face more difficulties when the input data impurity increases. Remarkably, TSAD-C consistently attains the highest F1, irrespective of changes in κ . This underlines our method’s denoising prowess, as it remains effective regardless of the diversity in available anomaly types.

Variability on The Anomaly Ratio. We investigate the robustness of TSAD-C by varying the anomaly ratio. Note that all anomaly types, i.e., $\kappa = 5$, are present within each subset of the dataset for this experiment. Figure 3 **(Right)** shows that TSAD-C exhibits consistent performance across different ratios of anomalies, reinforcing the demonstration of the Decontaminator’s effectiveness in TSAD-C. Meanwhile, unlike TSAD-C, the performance of other unsupervised methods tends to decline as normal data impurity increases.

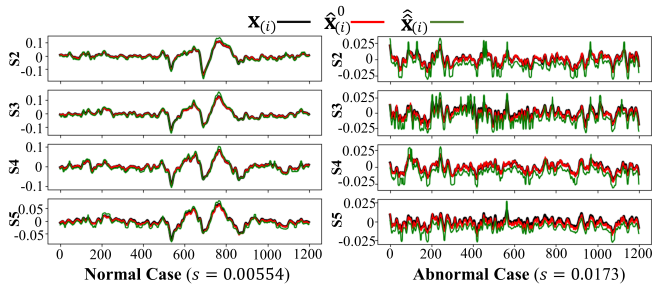


Figure 4: Comparison between normal and abnormal cases for the masked segment in DODH (S: Sensor). The masked strategy used is BoM. Each case includes $\mathbf{x}_{(i)}$, $\mathbf{x}_{(i)}^0$ and $\hat{\mathbf{x}}_{(i)}$.

3.4 Visualization of Normal Approximation

Figure 4 shows a visualization that compares the ground truth $\mathbf{x}_{(i)}$, decontaminated data $\mathbf{x}_{(i)}^0$, and reconstructed data $\hat{\mathbf{x}}_{(i)}$ of a masked segment of normal and abnormal samples in DODH. The segment of the $\mathbf{x}_{(i)}$ is masked to zeros, by applying BoM, before being processed by the Decontaminator. It is shown that $\mathbf{x}_{(i)}^0$ and $\hat{\mathbf{x}}_{(i)}$ fit $\mathbf{x}_{(i)}$ very well in the normal case, leading to a lower s . Meanwhile, there are significant fluctuations of $\mathbf{x}_{(i)}^0$ and $\hat{\mathbf{x}}_{(i)}$ compared to $\mathbf{x}_{(i)}$ in the abnormal case, resulting in a much higher s . This shows the effectiveness of TSAD-C in distinguishing anomalies from normal data.

3.5 Ablation Study

Certainly, handling contaminated data requires the indispensable inclusion of Module (1), i.e., the Decontaminator in TSAD-C. Excluding it would align the TSAD-C’s detection results with those of other unsupervised methods. Hence, we conduct ablation studies specifically focusing on Module (2), i.e., Long-range Variable Dependency Modeling, and Module (3), i.e., Anomaly Scoring, as shown in Table 3. RandBM is used in all experiments for these studies. The sign “-” denotes the exclusion of a component.

Module (2). The results are shown in the first and second rows of the Table, where Intra and Inter, respectively, denote the Intra-variable Modeling, and Inter-variable Modeling components. Note that, for this experiment, the anomaly score s_2 is computed using the non-removed block of Module (2), meaning that, for the first and second rows, s_2 is determined by Inter and Intra, respectively. The results highlight the superior performance achieved by capturing long-range intra-variable dependencies, showing that while Inter is also an important component, having Intra is often prioritized due to the nature of time-series data.

Module (3). The results are shown in the third and fourth rows of the Table. For this study, during training, all components of Modules (1) and (2) are available, whereas we exclude either s_1 or s_2 , respectively, obtained from Module (1) or Module (2) in the test phase. The results show that by removing either s_1 or s_2 , we observe a small drop in performance. This can be attributed to the fact that in the test phase, we still perform data decontamination using the Decontaminator module trained during the training phase. Such data decontamination in the test phase resembles a case where one

TSAD-C	Metric	ICBEB	DODH	TUSZ	
Module (2)	- Intra	F1	0.651	0.565	0.499
	- -	{Rec; APR}	{0.735; 0.738}	{0.637; 0.667}	{0.655; 0.598}
	- Inter	F1	0.686	0.622	0.535
- -	{Rec; APR}	{0.803; 0.759}	{0.762; 0.705}	{0.789; 0.639}	
Module (3)	- s_1	F1	0.706	0.637	0.517
	- -	{Rec; APR}	{0.856; 0.771}	{0.80; 0.716}	{0.745; 0.622}
	- s_2	F1	0.699	0.627	0.518
- -	{Rec; APR}	{0.818; 0.768}	{0.787; 0.709}	{0.712; 0.617}	
All	F1	0.707	0.652	0.545	
	{Rec; APR}	{0.841; 0.773}	{0.843; 0.728}	{0.830; 0.652}	

Table 3: The performance of individual components in TSAD-C and their combinations. The best F1 scores are denoted in bold.

Masking Type	Metric	ICBEB	DODH	TUSZ
RandM	F1	0.694	0.647	0.520
	{Rec; APR}	{0.825; 0.764}	{0.837; 0.724}	{0.793; 0.631}
RandBM	F1	0.707	0.652	0.545
	{Rec; APR}	{0.841; 0.773}	{0.843; 0.728}	{0.830; 0.652}
BoM	F1	0.669	0.623	0.531
	{Rec; APR}	{0.795; 0.747}	{0.806; 0.707}	{0.810; 0.640}

Table 4: Comparison between different masking strategies used in TSAD-C. The best F1 scores are denoted in bold.

performs the unsupervised anomaly detection of the clean test data. This experiment can be considered as a demonstration of the effectiveness of the Decontaminator.

Importantly, integrating all components together both in training and test phases (aka **All**) yields the best performance across all datasets, as shown in the last row of the Table, showcasing the synergistic complementarity of each component in enhancing the model’s ability to detect anomalies.

3.6 Effect of Masking Strategy

Table 4 demonstrates that the performance of TSAD-C remains largely consistent when utilizing either RandM, RandBM, or BoM, underscoring the effectiveness of our chosen masking techniques. Despite this consistency, noteworthy differences emerge, with RandBM showcasing the most optimal performance. This outcome may be attributed to introducing randomness into the masked time windows, which increases the level of robustness and adaptability to diverse patterns and variations in the data. Note that this adaptability is crucial for real-world applications where anomalies can manifest in diverse ways across sensors or data sources. RandBM emulates this inherent diversity, enabling the model to effectively learn and detect anomalies characterized by sensor-specific patterns, contributing to its overall efficacy.

4 Conclusion

This paper is the first attempt to provide a novel approach trained on contaminated data to detect anomalous observations in time-series data. The proposed method, called TSAD-C, consists of the Decontaminator, aimed at removing the potentially anomalous patterns in the training phase.

Given decontaminated data, we propose the Long-range Variable Dependency Modeling to capture long-range intra- and inter-variable dependencies and provide an approximation of purified input data. An Anomaly Scoring module is achieved by integrating the capability of the two modules. We demonstrate the outperformance of TSAD-C on three challenging physiological datasets compared to the existing methods.

References

- [Alcaraz and Strodthoff, 2022] Juan Miguel Lopez Alcaraz and Nils Strodthoff. Diffusion-based time series imputation and forecasting with structured state space models. *arXiv preprint arXiv:2208.09399*, 2022.
- [Carmona *et al.*, 2022] Chris U Carmona, Francois-Xavier Aubet, Valentin Flunkert, and Jan Gasthaus. Neural contextual anomaly detection for time series. In *International Joint Conference on Artificial Intelligence*, 2022.
- [Chen *et al.*, 2022] Wenchao Chen, Long Tian, Bo Chen, Liang Dai, Zhibin Duan, and Mingyuan Zhou. Deep variational graph convolutional recurrent network for multivariate time series anomaly detection. In *International Conference on Machine Learning*, pages 3621–3633. PMLR, 2022.
- [Davis and Goadrich, 2006] Jesse Davis and Mark Goadrich. The relationship between precision-recall and roc curves. In *Proceedings of the 23rd international conference on Machine learning*, pages 233–240, 2006.
- [Deng and Hooi, 2021] Ailin Deng and Bryan Hooi. Graph neural network-based anomaly detection in multivariate time series. In *Proceedings of the AAAI conference on artificial intelligence*, pages 4027–4035, 2021.
- [Du *et al.*, 2022] Xusheng Du, Jiong Yu, Zheng Chu, Lina Jin, and Jiaying Chen. Graph autoencoder-based unsupervised outlier detection. *Information Sciences*, 608:532–550, 2022.
- [Gao and Ribeiro, 2022] Jianfei Gao and Bruno Ribeiro. On the equivalence between temporal and static equivariant graph representations. In *International Conference on Machine Learning*, pages 7052–7076. PMLR, 2022.
- [Gu *et al.*, 2020] Albert Gu, Tri Dao, Stefano Ermon, Atri Rudra, and Christopher Ré. Hippo: Recurrent memory with optimal polynomial projections. *Advances in neural information processing systems*, 33:1474–1487, 2020.
- [Gu *et al.*, 2022] Albert Gu, Karan Goel, and Christopher Ré. Efficiently modeling long sequences with structured state spaces. In *International Conference on Learning Representations*, 2022.
- [Guillot *et al.*, 2020] Antoine Guillot, Fabien Sauvet, Emmanuel H Doring, and Valentin Thorey. Dream open datasets: Multi-scored sleep datasets to compare human and automated sleep staging. *IEEE transactions on neural systems and rehabilitation engineering*, 28(9):1955–1965, 2020.
- [Ho and Armanfard, 2023] Thi Kieu Khanh Ho and Narges Armanfard. Self-supervised learning for anomalous channel detection in eeg graphs: Application to seizure analysis. In *Proceedings of the AAAI Conference on Artificial Intelligence*, volume 37, pages 7866–7874, 2023.
- [Ho *et al.*, 2023] Thi Kieu Khanh Ho, Ali Karami, and Narges Armanfard. Graph-based time-series anomaly detection: A survey. *arXiv preprint arXiv:2302.00058*, 2023.
- [Hojjati *et al.*, 2023] Hadi Hojjati, Mohammadreza Sadeghi, and Narges Armanfard. Multivariate time-series anomaly detection with temporal self-supervision and graphs: Application to vehicle failure prediction. In *Joint European Conference on Machine Learning and Knowledge Discovery in Databases*, pages 242–259. Springer, 2023.
- [Jiang *et al.*, 2022] Xi Jiang, Jianlin Liu, Jinbao Wang, Qiang Nie, Kai Wu, Yong Liu, Chengjie Wang, and Feng Zheng. Softpatch: Unsupervised anomaly detection with noisy data. *Advances in Neural Information Processing Systems*, 35:15433–15445, 2022.
- [Katharopoulos *et al.*, 2020] Angelos Katharopoulos, Apoorv Vyas, Nikolaos Pappas, and Francois Fleuret. Transformers are rnns: Fast autoregressive transformers with linear attention. In *International Conference on Machine Learning*, pages 5156–5165. PMLR, 2020.
- [Khayati *et al.*, 2020] Mourad Khayati, Alberto Lerner, Zakhar Tymchenko, and Philippe Cudré-Mauroux. Mind the gap: an experimental evaluation of imputation of missing values techniques in time series. In *Proceedings of the VLDB Endowment*, volume 13, pages 768–782, 2020.
- [Kuan *et al.*, 2017] Chung-Ming Kuan, Christos Michalopoulos, and Zhijie Xiao. Quantile regression on quantile ranges—a threshold approach. *Journal of Time Series Analysis*, 38(1):99–119, 2017.
- [Li *et al.*, 2021] Zhihan Li, Youjian Zhao, Jiaqi Han, Ya Su, Rui Jiao, Xidao Wen, and Dan Pei. Multivariate time series anomaly detection and interpretation using hierarchical inter-metric and temporal embedding. In *Proceedings of the 27th ACM SIGKDD conference on knowledge discovery & data mining*, pages 3220–3230, 2021.
- [Lim *et al.*, 2021] Soon Hoe Lim, N Benjamin Erichson, Liam Hodgkinson, and Michael W Mahoney. Noisy recurrent neural networks. *Advances in Neural Information Processing Systems*, 34:5124–5137, 2021.
- [Liu *et al.*, 2018] Feifei Liu, Chengyu Liu, Lina Zhao, Xiangyu Zhang, Xiaoling Wu, Xiaoyan Xu, Yulin Liu, Caiyun Ma, Shoushui Wei, Zhiqiang He, et al. An open access database for evaluating the algorithms of electrocardiogram rhythm and morphology abnormality detection. *Journal of Medical Imaging and Health Informatics*, 8(7):1368–1373, 2018.
- [Pradhan *et al.*, 2022] Ashirbad Pradhan, Jiayuan He, and Ning Jiang. Hand gesture recognition and biometric authentication using a multi-day dataset. In *Intelligent Robotics and Applications: 15th International Conference, ICIRA 2022, Harbin, China, August 1–3, 2022, Proceedings, Part IV*, pages 375–385. Springer, 2022.

- [Shah *et al.*, 2018] Vinit Shah, Eva Von Weltin, Silvia Lopez, James Riley McHugh, Lillian Veloso, Meysam Golmohammadi, Iyad Obeid, and Joseph Picone. The temple university hospital seizure detection corpus. *Frontiers in neuroinformatics*, 12:83, 2018.
- [Shen *et al.*, 2020] Lifeng Shen, Zhuocong Li, and James Kwok. Timeseries anomaly detection using temporal hierarchical one-class network. *Advances in Neural Information Processing Systems*, 33:13016–13026, 2020.
- [Sohl-Dickstein *et al.*, 2015] Jascha Sohl-Dickstein, Eric Weiss, Niru Maheswaranathan, and Surya Ganguli. Deep unsupervised learning using nonequilibrium thermodynamics. In *International conference on machine learning*, pages 2256–2265. PMLR, 2015.
- [Strodthoff *et al.*, 2020] Nils Strodthoff, Patrick Wagner, Tobias Schaeffter, and Wojciech Samek. Deep learning for ecg analysis: Benchmarks and insights from ptb-xl. *IEEE Journal of Biomedical and Health Informatics*, 25(5):1519–1528, 2020.
- [Su *et al.*, 2019] Ya Su, Youjian Zhao, Chenhao Niu, Rong Liu, Wei Sun, and Dan Pei. Robust anomaly detection for multivariate time series through stochastic recurrent neural network. In *Proceedings of the 25th ACM SIGKDD international conference on knowledge discovery & data mining*, pages 2828–2837, 2019.
- [Tang *et al.*, 2021] Siyi Tang, Jared Dunnmon, Khaled Kamal Saab, Xuan Zhang, Qianying Huang, Florian Dubost, Daniel Rubin, and Christopher Lee-Messer. Self-supervised graph neural networks for improved electroencephalographic seizure analysis. In *International Conference on Learning Representations*, 2021.
- [Tang *et al.*, 2023] Siyi Tang, Jared A Dunnmon, Qu Liangqiong, Khaled K Saab, Tina Baykaner, Christopher Lee-Messer, and Daniel L Rubin. Modeling multivariate biosignals with graph neural networks and structured state space models. In *Conference on Health, Inference, and Learning*, pages 50–71. PMLR, 2023.
- [Vaswani *et al.*, 2017] Ashish Vaswani, Noam Shazeer, Niki Parmar, Jakob Uszkoreit, Llion Jones, Aidan N Gomez, Łukasz Kaiser, and Illia Polosukhin. Attention is all you need. *Advances in neural information processing systems*, 30, 2017.
- [Wagner *et al.*, 2023] Dennis Wagner, Tobias Michels, Florian CF Schulz, Arjun Nair, Maja Rudolph, and Marius Kloft. TimeSead: Benchmarking deep multivariate time-series anomaly detection. *Transactions on Machine Learning Research*, 2023.
- [Wei *et al.*, 2023] Yuanyuan Wei, Julian Jang-Jaccard, Wen Xu, Fariza Sabrina, Seyit Camtepe, and Mikael Boulic. Lstm-autoencoder-based anomaly detection for indoor air quality time-series data. *IEEE Sensors Journal*, 23(4):3787–3800, 2023.
- [Xu *et al.*, 2019] Keyulu Xu, Weihua Hu, Jure Leskovec, and Stefanie Jegelka. How powerful are graph neural networks? In *International Conference on Learning Representations*, 2019.
- [Zhang *et al.*, 2023] Hui Zhang, Zheng Wang, Zuxuan Wu, and Yu-Gang Jiang. Diffusionad: Denoising diffusion for anomaly detection. *arXiv preprint arXiv:2303.08730*, 2023.
- [Zhu *et al.*, 2021] Yanqiao Zhu, Weizhi Xu, Jinghao Zhang, Yuanqi Du, Jieyu Zhang, Qiang Liu, Carl Yang, and Shu Wu. A survey on graph structure learning: Progress and opportunities. *arXiv preprint arXiv:2103.03036*, 2021.